J. Plasma Phys. (2024), *vol*. 90, 905900201
Published by Cambridge University Press
doi:10.1017/S0022377824000217

Nonlinear electron scattering by electrostatic waves in collisionless shocks

Sergei R. Kamaletdinov[1,2,3,†], **Ivan Y. Vasko**[1,4] **and Anton V. Artemyev**[1,3]

[1]Space Research Institute of the Russian Academy of Sciences (IKI), 84/32 Profsoyuznaya Str., Moscow 117997, Russia

[2]Faculty of Physics, National Research University Higher School of Economics, 21/4 Staraya Basmannaya Ulitsa, Moscow 105066, Russia

[3]Department of Earth, Planetary, and Space Sciences, University of California, 595 Charles E Young Dr E, Los Angeles, CA 90095, USA

[4]William B. Hanson Center for Space Sciences, University of Texas at Dallas, 800 W Campbell Rd., Richardson, TX 75080, USA

(Received 11 October 2023; revised 31 January 2024; accepted 31 January 2024)

We present a theoretical analysis of electron pitch-angle scattering by ion-acoustic electrostatic fluctuations present in the Earth's bow shock and, presumably, collisionless shocks in general. We numerically simulate electron interaction with a single wave packet to demonstrate the scattering through phase bunching and phase trapping and quantify electron pitch-angle scattering in dependence on the wave amplitude and wave normal angle to the local magnetic field. The iterative mapping technique is used to model pitch-angle scattering of electrons by a large number of wave packets, which have been reported in the Earth's bow shock. Assuming that successive electron scatterings are not correlated, we revealed that the long-term dynamics of electrons is diffusive. The diffusion coefficient depends on the ratio Φ_0/W between the wave packet amplitude and electron energy, $D \propto (\Phi_0/W)^\nu$. A quasi-linear scaling ($\nu \approx 2$) is observed for sufficiently small wave amplitudes, $\Phi_0 \lesssim 10^{-3}W$, while the diffusion is nonlinear ($1 < \nu < 2$) above this threshold. We show that pitch-angle diffusion of $\lesssim$1 keV electrons in the Earth's bow shock can be nonlinear. The corresponding diffusion coefficient scales with the intensity E_w^2 of the electrostatic fluctuations in a nonlinear fashion, $D \propto E_w^\nu$ with $\nu < 2$, while its expected values in the Earth's bow shock are $D \sim 0.1$–$100\ (T_e/W)^{\nu-1/2}$ rad^2 s^{-1}. We speculate that in the Earth's quasi-perpendicular bow shock the stochastic shock drift acceleration mechanism with pitch-angle scattering provided by the electrostatic fluctuations can contribute to the acceleration of thermal electrons up to approximately 1 keV. The potential effects of a finite perpendicular coherence scale of the wave packets on the efficiency of electron scattering are discussed.

Keywords: plasma nonlinear phenomena, plasma waves, plasma simulation

1. Introduction

The mechanisms of electron heating and acceleration in collisionless shock waves are still not entirely resolved (e.g. Ghavamian *et al.* 2013; Krasnoselskikh *et al.* 2013;

† Email address for correspondence: sergei2033@g.ucla.edu

Amano *et al.* 2022). The understanding of these mechanisms would substantially advance the interpretation of remote observations of astrophysical shocks in supernova remnants and galaxy clusters (Markevitch & Vikhlinin 2007; Ghavamian *et al.* 2013; Raymond *et al.* 2023). Even though the Earth's bow shock is not identical to astrophysical shocks, it is still a perfect natural laboratory for probing plasma processes around supercritical collisionless shocks using *in situ* observations. The early spacecraft measurements in the Earth's bow shock demonstrated that the macroscopic electric field, which occurs because of different electron and ion dynamics, should provide a leading contribution to the electron heating (Scudder 1995). The modern spacecraft measurements showed, however, that electron heating is typically non-adiabatic (Gedalin *et al.* 2023; Johlander *et al.* 2023) and revealed electron acceleration up to tens of keV (Gosling *et al.* 1989; Oka *et al.* 2006). The non-adiabatic heating and superthermal electrons indicate that electric and magnetic field fluctuations must be involved in electron heating and acceleration processes in collisionless shocks. According to numerical simulations, electron pitch-angle scattering produced by electric and magnetic field fluctuations observed in the Earth's bow shock can indeed result in non-adiabatic heating (Vasko *et al.* 2018*b*; Oka *et al.* 2019; Gedalin 2020; Artemyev *et al.* 2022) and acceleration through the stochastic shock drift acceleration (SSDA) mechanism (Amano *et al.* 2020, 2022). The contribution of different electric and magnetic field fluctuations to electron heating and acceleration processes around collisionless shocks is currently actively investigated.

Spacecraft measurements revealed various electromagnetic and electrostatic fluctuations in the Earth's bow shock (e.g. Gurnett 1985; Wilson *et al.* 2014). The most intense among the electromagnetic fluctuations are fast magnetosonic and whistler-mode waves produced by, respectively, ion and electron instabilities (Oka *et al.* 2017, 2019; Page *et al.* 2021; Lalti *et al.* 2022). The electrostatic fluctuations typically have broadband power spectra and, particularly, consist of electrostatic solitary waves and wave packets interpreted in terms of, respectively, ion or electron phase space holes and ion-acoustic waves (Fuselier & Gurnett 1984; Balikhin *et al.* 2005; Hull *et al.* 2006; Vasko *et al.* 2020, 2022; Wang *et al.* 2020, 2021; Kamaletdinov *et al.* 2022). Note that electron cyclotron harmonics coupled with ion-acoustic waves also contribute to electrostatic fluctuations in the Earth's bow shock (Breneman *et al.* 2013; Wilson *et al.* 2014; Muschietti & Lembège 2017). The recent analysis of spacecraft measurements around the Earth's quasi-perpendicular bow shock showed that superthermal electron fluxes up to a few tens of keV can be produced through the SSDA mechanism with pitch-angle scattering provided by electromagnetic fluctuations (Amano *et al.* 2020). While the electromagnetic fluctuations can indeed provide efficient scattering of thermal and superthermal electrons, recent theoretical computations demonstrated that pitch-angle scattering by electrostatic fluctuations can also be efficient below approximately 1 keV (Vasko *et al.* 2018*b*; Kamaletdinov *et al.* 2022). In particular, the computations showed that pitch-angle scattering by electrostatic solitary waves can result in acceleration of thermal electrons up to a few hundred eV provided that the observed electrostatic wave power corresponds solely to these electrostatic structures (Kamaletdinov *et al.* 2022). In reality, electrostatic solitary waves have a relatively low occurrence and the observed electrostatic wave power in the Earth's bow shock is predominantly due to electrostatic wave packets (Breneman *et al.* 2013; Wang *et al.* 2020, 2021; Vasko *et al.* 2020, 2022). This stimulates the present analysis of electron pitch-angle scattering by electrostatic wave packets present in the Earth's bow shock and, presumably, collisionless shocks in general.

The recent measurements aboard the Magnetospheric Multiscale spacecraft (Burch *et al.* 2016) have allowed the most detailed analysis of electrostatic fluctuations in the Earth's bow shock. Figure 1 demonstrates several electrostatic wave packets observed aboard the

https://doi.org/10.1017/S0022377824000217 Published online by Cambridge University Press

Magnetospheric Multiscale spacecraft around the ramp of the Earth's quasi-perpendicular bow shock. The bottom panels demonstrate electrostatic wave packets with amplitudes up to a few hundred mV m^{-1}, plasma frame speeds of approximately a hundred km s^{-1}, which is around the local ion-acoustic speed, and typical wavelengths of approximately a few hundred metres, which is approximately a few tens of local Debye lengths. Importantly, these electrostatic wave packets have the electric field oriented quasi-parallel, oblique or quasi-perpendicular to the local magnetic field and amplitudes of the electrostatic potential of up to a few tens of volts, which is approximately 1 %–20 % of the local electron temperature. Similar properties are actually typical of all other electrostatic wave packets observed in this Earth bow shock crossing (Vasko *et al.* 2022): wavelengths from a few tens to a few hundred Debye lengths, amplitudes of a substantial fraction of the local electron temperature and electric fields oriented at arbitrary angles to the local magnetic field. Quantifying electron scattering by these electrostatic fluctuations is not elementary, since quasi-linear theory may not be applicable for the observed large amplitudes (e.g. Omura *et al.* 1991, 2015; Albert, Meredith & Horne 2009; Shklyar & Matsumoto 2009).

In this study we apply a probabilistic approach (Artemyev *et al.* 2021; Lukin, Artemyev & Petrukovich 2021; Zhang *et al.* 2022) to quantify electron scattering by electrostatic fluctuations reported in the Earth's bow shock and demonstrate that electron pitch-angle scattering is diffusive, but overall not described within quasi-linear theory. The revealed scattering rates are used to evaluate the efficiency of the electrostatic fluctuations in producing superthermal electron fluxes in the Earth's bow shock. The paper is organized as follows. In § 2 we introduce a model electrostatic wave packet and demonstrate several typical electron trajectories. In § 3 we consider pitch-angle scattering of electron ensembles by wave packets of different amplitudes and trace a long-term evolution of electron pitch angles using a stochastic iterative mapping technique. The latter emulates electron scattering by a large number of electrostatic wave packets, whose parameters are distributed according to spacecraft observations in the Earth's bow shock. In § 4 we compute the pitch-angle diffusion coefficient and its scaling with electron energy and the amplitude of the electrostatic wave packets. In § 5 we discuss our results and estimate the efficiency of the electrostatic fluctuations in producing superthermal electron fluxes through the SSDA mechanism.

2. Basic equations and main regimes of electron scattering

We investigate electron scattering by electrostatic wave packets propagating obliquely to the local magnetic field. We introduce a Cartesian coordinate system with the z-axis aligned with a uniform local magnetic field B_0, the x-axis perpendicular to the wave propagation direction and the y-axis completing the right-handed system. The electrostatic wave packet is assumed to be planar and described by a one-dimensional electrostatic potential $\Phi = \Phi(z\cos\theta + y\sin\theta)$, where θ is the wave normal angle. The assumption of planarity certainly oversimplifies the actual structure of wave packets in the Earth's bow shock, in § 4, we will discuss the potential effects of a finite perpendicular coherence scale. The dimensionless equations describing the electron dynamics can be written as follows:

$$\left.\begin{aligned} \dot{V}_x &= -\Omega V_y, \\ \dot{V}_y &= \partial\Phi/\partial y + \Omega V_x, \\ \dot{V}_z &= \partial\Phi/\partial z, \end{aligned}\right\} \tag{2.1}$$

where the spatial coordinates are normalized to the electron Debye length $\lambda_D = (T_e/4\pi n_e e^2)^{1/2}$, the electron velocity V is normalized to electron thermal speed

https://doi.org/10.1017/S0022377824000217 Published online by Cambridge University Press

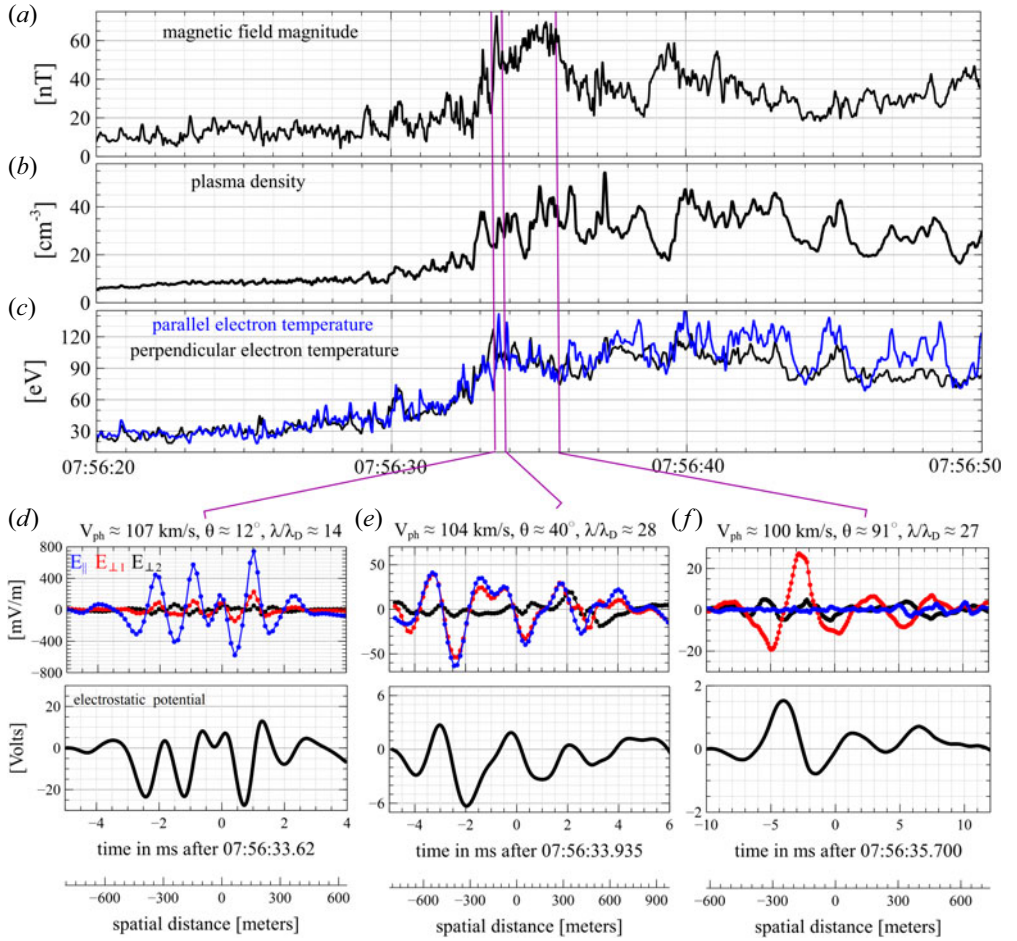

FIGURE 1. The demonstration of electrostatic wave packets observed on 4 November 2015 aboard the Magnetospheric Multiscale spacecraft around the Earth's quasi-perpendicular bow shock (only MMS3 measurements are shown here): (*a*) the magnetic field magnitude measured at 128 Samples s^{-1} by digital and analogue fluxgate magnetometers (Russell *et al.* 2016), (*b*) electron density and (*c*) electron temperatures (parallel and perpendicular) measured at 30 ms resolution by the Fast Plasma Investigation instrument (Pollock *et al.* 2016), (*d–f*) electric field waveforms of electrostatic wave packets propagating at different angles to the local magnetic field, where electric field measurements are provided at 8192 samples s^{-1} by the axial double probe (Ergun *et al.* 2016) and spin-plane double probe (Lindqvist *et al.* 2016). For each wave packet we present the electric field in local magnetic field-aligned coordinates and the electrostatic potential computed by integrating over time the electric field multiplied by the wave propagation velocity in the spacecraft frame. The bottom axes in panels (*d–f*) convert temporal scale into spatial scale by multiplying with the revealed propagation velocity. Note that the spacecraft frame velocities of these waves were estimated using measurements of the double-probe instrument aboard the Magnetospheric Multiscale spacecraft. The corresponding methodology and a more detailed analysis of this Earth bow shock crossing can be found in Vasko *et al.* (2022). In panels (*d–f*) we also present the plasma frame speed $V_{\rm ph}$, wave normal angle θ with respect to the local magnetic field and typical wavelength λ in units of local electron Debye length λ_D.

https://doi.org/10.1017/S0022377824000217 Published online by Cambridge University Press

$V_{\rm th} = (T_e/m_e)^{1/2}$, the time variable t is normalized to the inverse plasma frequency, the electrostatic potential Φ is normalized to the electron temperature T_e and $\Omega = \omega_{\rm ce}/\omega_{\rm pe}$ is the ratio between the electron cyclotron frequency $\omega_{\rm ce} = eB_0/m_e c$ and the electron plasma frequency $\omega_{\rm pe} = (4\pi n_e e^2/m_e)^{1/2}$. Note that n_e is the plasma density, $-e$ and m_e are the electron charge and mass. In what follows, we assume $\Omega = 10^{-2}$, which is typical of the Earth's bow shock. Note that a finite background magnetic field ($\Omega \neq 0$) is crucial for electron scattering to occur. The quasi-linear theory predicts that pitch-angle scattering does not occur in the absence of a background magnetic field (e.g. Kamaletdinov *et al.* 2022). Therefore, nonlinear scattering is also expected to depend on the background magnetic field.

We use the following model for the electrostatic potential of electrostatic wave packets observed in the Earth's bow shock:

$$\Phi = \Phi_0\, e^{-\zeta^2/2l^2} \cos(k\zeta), \tag{2.2}$$

where Φ_0 and l are the amplitude and typical half-width of the wave packet, k is the typical wavenumber and $\zeta = z\cos\theta + y\sin\theta$. Electrostatic wave packets in the Earth's bow shock usually comprise a few wavelengths, while the observed wavelengths are around a few tens of Debye lengths (figure 1). Adopting the parameters observed in the Earth's bow shock, we assume $kl = 9$ and $k = 2\pi/\lambda = 2\pi/20\lambda_D$. The plasma frame velocity of the electrostatic waves is typically around the local ion-acoustic speed, that is well below the local electron thermal speed. Since this study is focused on electron pitch-angle scattering, we assume wave packets with zero velocity in the plasma frame. The inclusion of finite, but small compared with the electron thermal speed, wave velocities would not substantially affect pitch-angle scattering and only lead to insignificant scattering in energy (§ 4).

Figure 2 shows typical electron trajectories obtained by numerical integration of (2.1) for a relatively intense wave packet with amplitude of $\Phi_0 = 0.1$ and wave normal angle of $\theta = 50^\circ$. The initial conditions correspond to electrons with identical initial energies of $W = 2$ and pitch angles of $\alpha_0 = 30^\circ$, but different initial gyrophases, $\varphi \in [0, 2\pi]$. The unperturbed electron trajectory is a helix with $x = -\rho_L \sin(\Omega t + \varphi)$, $y = \rho_L \cos(\Omega t + \varphi)$ and $z = z_0 + (2W)^{1/2} t\cos(\alpha_0)$, where $\rho_L = (2W/\Omega^2)^{1/2}\sin\alpha_0$ denotes the electron gyroradius. We recall that $\Omega = \omega_{\rm ce}/\omega_{\rm pe}$, while the electron energy W and time variable t have been normalized to the electron temperature and the inverse electron plasma frequency, respectively.

Panels (*a–f*) show a couple of numerically integrated electron trajectories in the yz, V_xV_y and V_zV_x planes. The corresponding evolution of the electron pitch angles is demonstrated in panel (*g*). The electrons are initially far away from the wave packet and manage to perform at least one full cyclotron rotation before entering the region occupied by the wave packet at $t \approx 500$. The resonant interaction occurs around $t \approx 500$ and manifests itself in the pitch-angle evolution demonstrated in panel (*g*). We trace electron trajectories until they leave the region occupied by the wave packet and the pitch angle saturates at its final value $\alpha_f = \alpha_0 + \Delta\alpha$. Panel (*g*) presents the pitch-angle evolution for another 29 electrons with randomly selected initial gyrophases. Most of the electrons are only weakly scattered with pitch-angle jumps $\Delta\alpha$ within a few degrees. The electron trajectory presented in panels (*a–c*) corresponds to $\Delta\alpha \approx -2.2^\circ$ and exemplifies weak scattering of most of the electrons. For one of the electrons the pitch angle changes substantially, however, $\Delta\alpha \approx 20^\circ$, and the effect of this pitch-angle variation can be observed in the V_xV_y plane shown in panel (*d*).

The physical reason for this large pitch-angle jump can be revealed by inspecting electron trajectories in the $(\zeta, \dot{\zeta})$ phase space, where $\zeta = z\cos\theta + y\sin\theta$ and

https://doi.org/10.1017/S0022377824000217 Published online by Cambridge University Press

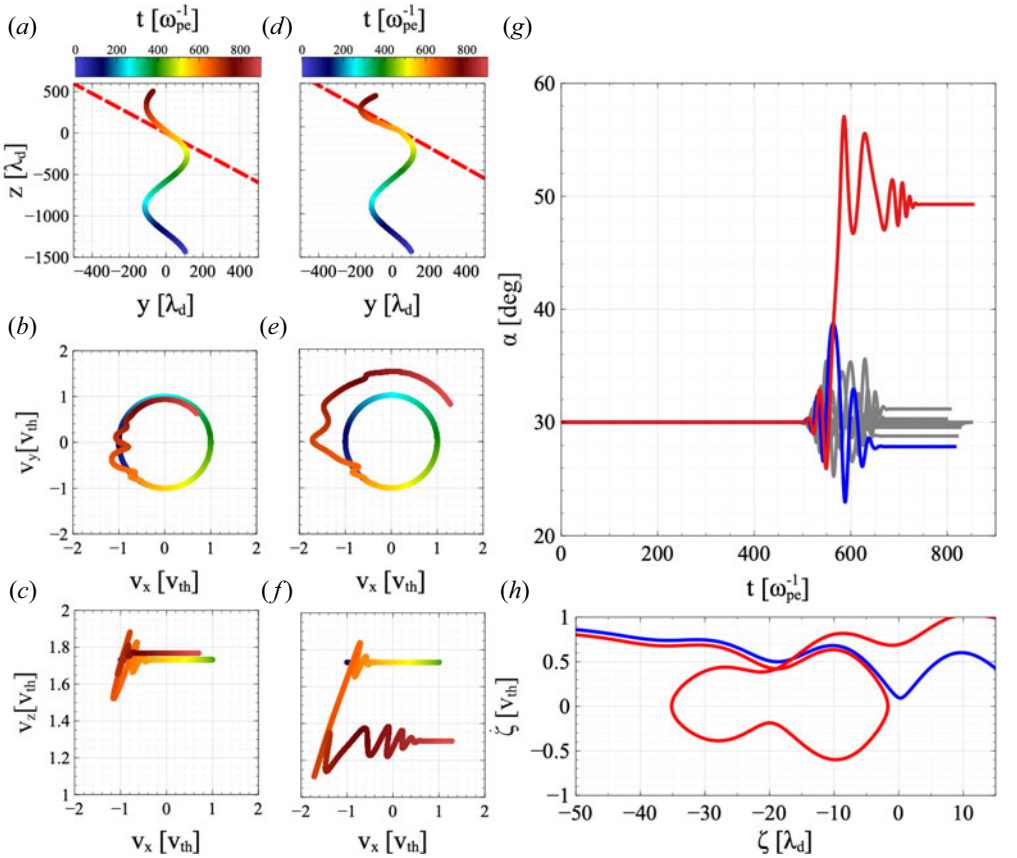

FIGURE 2. Electron trajectories obtained by numerical integration of (2.1) for a wave packet with amplitude $\Phi_0 = 0.1$ propagating obliquely at angle $\theta = 50^\circ$ to the local magnetic field directed along the z-axis. The numerical integration was done for electrons with identical initial energy $W = 2$ and pitch angle $\alpha_0 = 30^\circ$, but different gyrophases $\varphi \in [0, 2\pi]$. Panels (a–c) show projections of the electron trajectory corresponding to the initial gyrophase of $\varphi = 1.9845$ in the yz, V_xV_y and V_xV_z planes, where the time is indicated by colour. Panels (d–f) demonstrate similar projections of the electron trajectory corresponding to a slightly different initial gyrophase of $\varphi = 2.0451$. Panel (g) shows temporal pitch-angle evolution for an ensemble of 29 electrons with randomly chosen initial gyrophases: the blue line highlights the electron trajectory with $\varphi = 1.9845$ that was presented in panels (a–c), the red line stands for the electron trajectory with $\varphi = 2.0451$ that was shown in panels (d–f) while grey lines show trajectories of the other 27 electrons from the ensemble. Panel (h) shows the projection of the two highlighted trajectories in the $(\zeta, \dot{\zeta})$ phase space, where $\zeta = z\cos\theta + y\sin\theta$ and $\dot{\zeta} = V_z\cos\theta + V_y\sin\theta$.

$\dot{\zeta} \equiv \mathrm{d}\zeta/\mathrm{d}t = V_z\cos\theta + V_y\sin\theta$. Panel ($h$) presents electron trajectories in the $(\zeta, \dot{\zeta})$ phase space and shows that the trajectory corresponding to $\Delta\alpha \approx -2.2^\circ$ crosses the resonance $\dot{\zeta} \approx 0$ once, while the trajectory corresponding to $\Delta\alpha \approx 20^\circ$ is trapped in resonance and crosses $\dot{\zeta} \approx 0$ twice. Panel (d) shows that, in the latter case, the magnitude of velocity V_x significantly increases from $|V_x| \approx 0.9$ to approximately 1.8 at the expense of the $|V_z|$ decrease, which results in pitch-angle variation. The electron trajectories shown in panel (h) exemplify phase bunching and phase trapping, which are the fundamental effects of nonlinear wave–particle resonant interaction (e.g. Nunn 1971; Omura *et al.* 1991;

https://doi.org/10.1017/S0022377824000217 Published online by Cambridge University Press

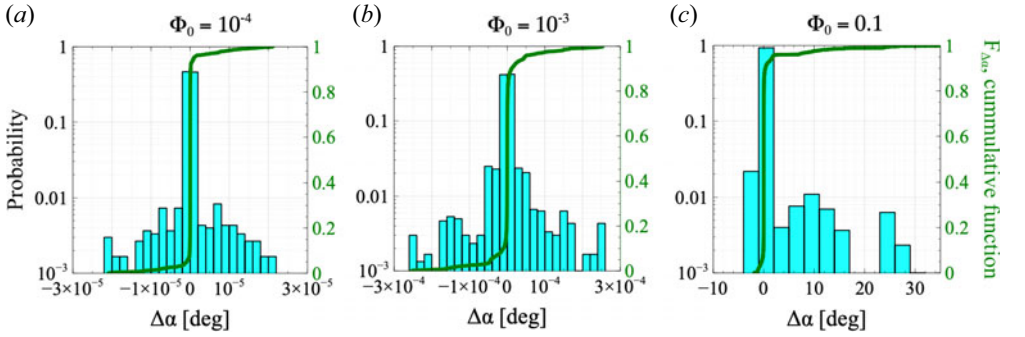

FIGURE 3. Probability and corresponding cumulative distributions of electron pitch-angle jumps $\Delta\alpha$ computed numerically for wave packets of different amplitudes: (*a*) $\Phi_0 = 10^{-4}$, (*b*) $\Phi_0 = 10^{-3}$ and (*c*) $\Phi_0 = 0.1$. Each distribution was obtained by numerically integrating trajectories of 3000 electrons with identical initial energies of $W = 2$ and pitch angles of $\alpha_0 = 30^\circ$, but randomly selected initial gyrophases.

Shklyar & Matsumoto 2009): phase trapping corresponds to particle oscillations around the resonance and substantial scattering, whereas phase bunching corresponds to a single resonant interaction and relatively weak scattering.

Figure 3 presents the analysis of electron scattering by wave packets of various amplitudes, $\Phi_0 = 10^{-4}$, 10^{-3} and 0.1, demonstrating that electron scattering depends not only on the electron initial conditions but also on the wave parameters. Panels (*a–c*) demonstrate the probability distributions of pitch-angle jumps $\Delta\alpha$ obtained by tracing 3000 electrons with identical initial energies of $W = 2$ and pitch angles of $\alpha_0 = 30^\circ$, but randomly distributed initial gyrophases. The corresponding cumulative distributions $F_{\Delta\alpha}$ are demonstrated as well. We expect that, for small-amplitude wave packets, pitch-angle jumps should be linearly proportional to the wave amplitude, $\Delta\alpha \propto \Phi_0$, because in this case the scattering can be quantified along unperturbed electron trajectories (Walt 1994; Vasko *et al.* 2017, 2018*a*). At sufficiently large amplitudes, the linear scaling is expected to break, because electron trajectories are significantly perturbed by the wave packet and the approximation of unperturbed trajectories does not apply. Panels (*a*,*b*) show that, at small amplitudes, a tenfold increase in amplitude indeed results in an approximately tenfold increase in the magnitude of pitch-angle jumps, while, overall, the probability distribution of these jumps does not change. In contrast, panel (*c*) shows that the scattering at large amplitudes leads to a substantially different probability distribution of pitch-angle jumps. The qualitatively different scattering at larger amplitudes is due to a larger contribution of electrons scattered through phase trapping.

3. Generalized diffusion rates

The scattering of an electron ensemble due to single interaction with a wave packet is entirely described by the cumulative distribution $F_{\Delta\alpha}$ of pitch-angle jumps $\Delta\alpha$. The cumulative distribution is computed numerically using an ensemble of electrons with uniformly distributed initial gyrophases: $F_{\Delta\alpha}(x|\alpha_0) \equiv N(\Delta\alpha < x)/N_0$, where N_0 is the total number of all the traced electrons, whose initial pitch angles are identical and equal α_0, while $N(\Delta\alpha < x)$ is the number of electrons with $\Delta\alpha < x$. To quantify electron scattering by a large number of successively encountered wave packets, we will assume that successive pitch-angle jumps are not correlated and describe the long-term electron scattering by incorporating the numerically computed cumulative distribution $F_{\Delta\alpha}$ into the

https://doi.org/10.1017/S0022377824000217 Published online by Cambridge University Press

stochastic iterative mapping technique (e.g. Artemyev *et al.* 2021; Lukin *et al.* 2021). The implementation of this technique for electrons of a fixed energy requires the distribution $F_{\Delta\alpha}$ to be computed for a broad range of initial pitch angles. These probability distributions need to be also computed for wave packets with different wave normal angles θ and amplitudes Φ_0, because wave packets successively encountered by electrons in a shock transition region are expected to be different. We assume, however, that the electrostatic potential of the different wave packets is still described by (2.2) with $kl = 9$ and $k = 2\pi/20\lambda_D$, as in the previous section.

Using the numerically obtained cumulative distribution, we generate a random variable $\Delta\alpha$ satisfying the numerically evaluated probability distribution function. This is accomplished by introducing random variable $\tilde{f}$ with a uniform distribution within [0, 1] and generating random variable $\Delta\alpha = F^{-1}_{\Delta\alpha}(\tilde{f}|\alpha_0)$. Since the random variable $\Delta\alpha$ depends on the initial pitch angle α_0, we use a set of 60 initial pitch angles uniformly distributed within [0°, 180°] to numerically compute a series of corresponding cumulative distributions $F_{\Delta\alpha}(x|\alpha_0)$ and random variables $\Delta\alpha(\alpha_0)$. Using interpolation, we obtain a continuous set of random variables $\Delta\alpha(\alpha_0)$ defined for arbitrary initial pitch angle α_0.

The cumulative distribution $F_{\Delta\alpha}(x|\alpha_0)$ and corresponding random variables $\Delta\alpha(\alpha_0)$ depend on electron energy W and wave packet parameters used in the numerical computations. Since electrostatic waves in the Earth's bow shock propagate at various angles to the local magnetic field (figure 1), we use $\{\theta_k\}_{k=1,\ldots,8} = \{10^\circ, \ldots, 80^\circ\}$ to compute a series of random variables $\{\Delta\alpha(\alpha_0|\theta_k)\}_{k=1,\ldots,8}$, where $\Delta\alpha(\alpha_0|\theta_k)$ is actually a shorthand for $\Delta\alpha(\alpha_0|\theta_k, \Phi_0, W)$. Since only a few studies of electrostatic waves have been carried out as yet, the realistic probability distribution of the wave normal angle θ is unknown. Therefore, we have to assume some model distribution $f(\theta)$ for wave packets encountered by electrons in the shock transition region. Here, $\int_a^b f(\theta)\,\mathrm{d}\theta$ is the probability of having $a < \theta < b$ and the probability distribution is normalized to unity, $\int_0^\pi f(\theta)\,\mathrm{d}\theta = 1$. A uniform distribution on a sphere would be $f(\theta) \propto \sin\theta$. We will use a model distribution $f(\theta) \propto \cos^2(2\theta)$ corresponding to a larger occurrence of quasi-parallel and quasi-perpendicular wave packets, but also test several other distributions, $f(\theta) \propto \cos^5\theta$ and $f(\theta) \propto \sin\theta$, emulating predominantly parallel and oblique propagation, respectively.

The set of random variables $\{\Delta\alpha(\alpha_0|\theta_k)\}_{k=1,\ldots,8}$ along with the wave normal angle distribution $f(\theta)$ allows modelling of pitch-angle scattering of electron ensembles with a given energy W by a large number of wave packets with a fixed amplitude Φ_0. Neglecting correlations between successive interactions, we obtain the following stochastic iterative mapping:

$$\alpha^{(i)}_{n+1} = \alpha^{(i)}_n + \Delta\alpha(\alpha^{(i)}_n|\theta), \tag{3.1}$$

where $\alpha^{(i)}_n$ stands for the pitch angle of the ith electron in the ensemble after interaction with n wave packets, whose wave normal angle θ is selected randomly among $\{\theta_k\}_{k=1,\ldots,8}$ according to the model distribution $f(\theta)$. Initial pitch angels $\alpha^{(i)}_0$ are selected randomly from the interval [0°, 180°].

Figure 4 shows the typical pitch-angle evolution computed using (3.1) for four electrons with randomly selected initial pitch angles. We demonstrate the evolution of electron pitch angles resulting from the scattering by small- and large-amplitude wave packets, $\Phi_0 = 0.001$ and $\Phi_0 = 0.1$. In the former case, the pitch-angle evolution is dominated by relatively small pitch-angle jumps and the overall behaviour resembles classical diffusion. The scattering is different in the case of the large-amplitude wave packets, since in addition to small pitch-angle jumps, there are infrequent jumps of a few tens of degrees. These

https://doi.org/10.1017/S0022377824000217 Published online by Cambridge University Press

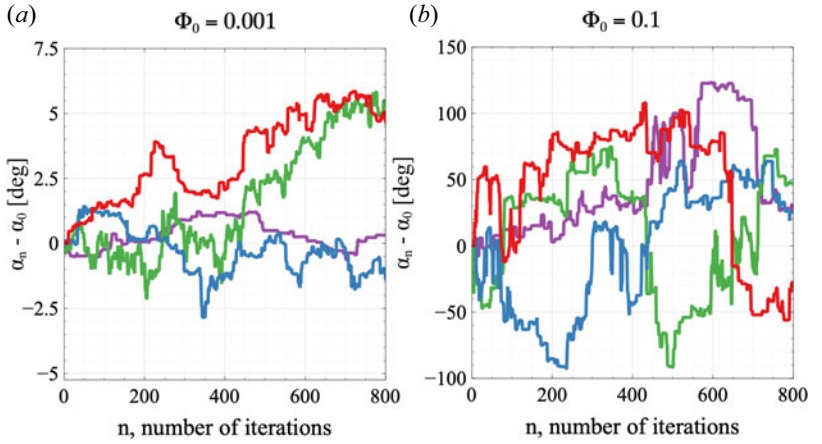

FIGURE 4. The typical pitch-angle evolution caused by electron scattering by a large number of electrostatic wave packets and modelled using (3.1). The energy of all the electrons is $W = 2$. The pitch-angle evolution is demonstrated for wave packets with amplitudes of (*a*) $\Phi_0 = 0.001$ and (*b*) $\Phi_0 = 0.1$. A single iteration corresponds to a single scattering by a wave packet, whose wave normal angle is chosen randomly according to the model distribution function $f(\theta) \propto \cos^2(2\theta)$.

significant pitch-angle jumps certainly correspond to phase trapping, demonstrated, for example, in figure 2.

The pitch-angle evolution can be described within quasi-linear diffusion theory (Vedenov, Velikhov & Sagdeev 1962; Kennel & Engelmann 1966) if the mean-square deviation $\sigma^2_{\Delta\alpha_n}$ scales linearly with time or, equivalently, with the number of resonant interactions. This scaling relation is expected to be violated for scattering by large-amplitude waves (Neishtadt, Chaikovskii & Chernikov 1991; Artemyev *et al.* 2016). Below, we introduce a numerical approach that allows us to test whether electron scattering by electrostatic wave packets observed in the Earth's bow shock can be described within quasi-linear diffusion theory.

Figure 5 demonstrates the scaling relation of $\sigma^2_{\Delta\alpha_n}$ with the number of resonant interactions n for electrons with an initial energy of $W = 5$ and wave packets with the wave normal angle distribution $f(\theta) \propto \cos^2(2\theta)$. For every fixed amplitude Φ_0 we used (3.1) to trace 10^4 electrons with initial pitch angles distributed uniformly within $[0^\circ, 180^\circ]$. For the ith electron with initial pitch angle $\alpha_0^{(i)}$ we follow the scheme demonstrated in figure 4 to generate a trajectory $\alpha_n^{(i)}$. The ensemble of all the electron trajectories $\{\alpha_n^{(i)}\}$ allows us to compute the mean-square deviation $\sigma^2_{\Delta\alpha_n} = \langle(\alpha_n^{(i)} - \alpha_0^{(i)})^2\rangle - \langle\alpha_n^{(i)} - \alpha_0^{(i)}\rangle^2$, where the brackets denote averaging over the 10^4 electrons. Panel (*a*) demonstrates $\sigma^2_{\Delta\alpha_n}$ vs n obtained for wave packets of various amplitudes. The power-law fitting revealed that, for all the considered amplitudes, we have $\sigma^2_{\Delta\alpha_n} \propto n$, which allowed us to introduce the diffusion rate D^* in units of rad^2 per interaction, $\sigma^2_{\Delta\alpha_n} = D^* \cdot n$. Note that the diffusion rate D^* is averaged over and is, hence, independent of the initial pitch angle α_0. Panel (*b*) shows the dependence of D^* on the wave amplitude Φ_0. For small amplitudes of $\Phi_0 \lesssim 10^{-2}$ we observe the classical scaling $D_* \propto \Phi_0^2$, consistent with predictions of the quasi-linear diffusion theory (Vedenov *et al.* 1962; Kennel & Engelmann 1966). For larger wave amplitudes $\Phi_0 \gtrsim 10^{-2}$, the diffusion coefficient deviates from quasi-linear diffusion theory. The compensated diffusion rates D^*/Φ_0^2 in panel (*c*) confirm that $D_* \propto \Phi_0^2$ below

https://doi.org/10.1017/S0022377824000217 Published online by Cambridge University Press

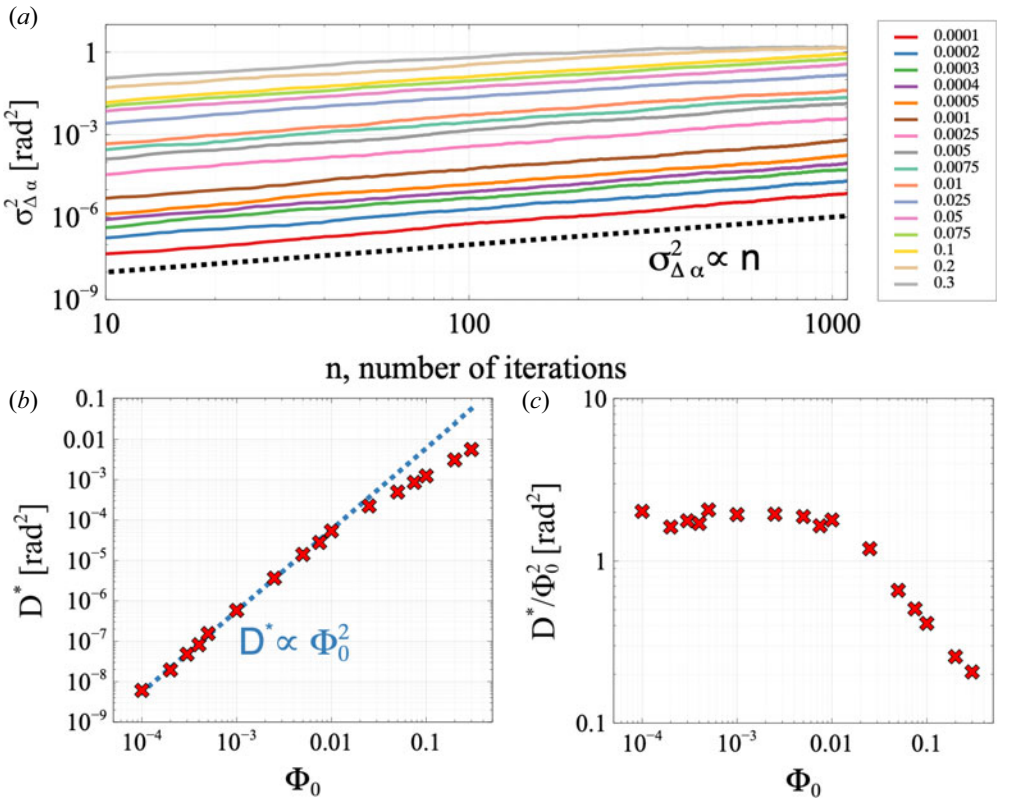

FIGURE 5. The evaluation of the diffusion rate D^* in units of rad^2 per interaction resulting from the modelling accomplished using (3.1). Note that this diffusion rate is averaged over and, hence, independent of the initial pitch angle. The electron energy is $W = 5$ and the distribution of wave packets in wave normal angle is $f(\theta) \propto \cos^2(2\theta)$. Panel (*a*) presents the mean-square deviation $\sigma^2_{\Delta\alpha_n}$ of the electron pitch angle computed by averaging over 10^4 electrons vs the number of resonant interactions n. The curves of different colours correspond to scattering by wave packets of different amplitudes Φ_0 indicated in the panel. The dotted black line shows $\sigma^2_{\Delta\alpha_n} \propto n$ for reference. Panel (*b*) presents the dependence of the diffusion rate D^* on wave amplitude Φ_0; the dotted blue line shows the scaling $D^* \propto \Phi_0^2$ expected from quasi-linear diffusion. Panel (*c*) presents the dependence of compensated diffusion rates D^*/Φ_0^2 on wave amplitude Φ_0.

the threshold of $\Phi_0 \approx 10^{-2}$, while the dependence is weaker, $D^* \propto \Phi_0^\nu$ with $\nu < 2$, above this threshold.

The analysis presented above was carried out for electrons with an initial energy of $W = 5$, while the critical property is the dependence of the diffusion rate D^*, not only on the wave amplitude, but also on the electron energy. It turned out that the diffusion rate D^* actually depends on the ratio between the wave amplitude and electron energy. To demonstrate this, we evaluated the diffusion rate D^* for a wide range of initial energies and wave amplitudes, $W \in [1, 100]$, and $\Phi_0 \in [10^{-4}, 0.2]$, which totals 48 values for the Φ_0/W ratio.

Figure 6 demonstrates that the diffusion rate D^* indeed depends only on the ratio Φ_0/W. Panels (*a–c*) demonstrate the results for wave packets with different wave normal angle distributions, $f(\theta) \propto \cos^2(2\theta)$, $\cos^5\theta$ and $\sin\theta$. The profiles of D^* vs Φ_0/W well

https://doi.org/10.1017/S0022377824000217 Published online by Cambridge University Press

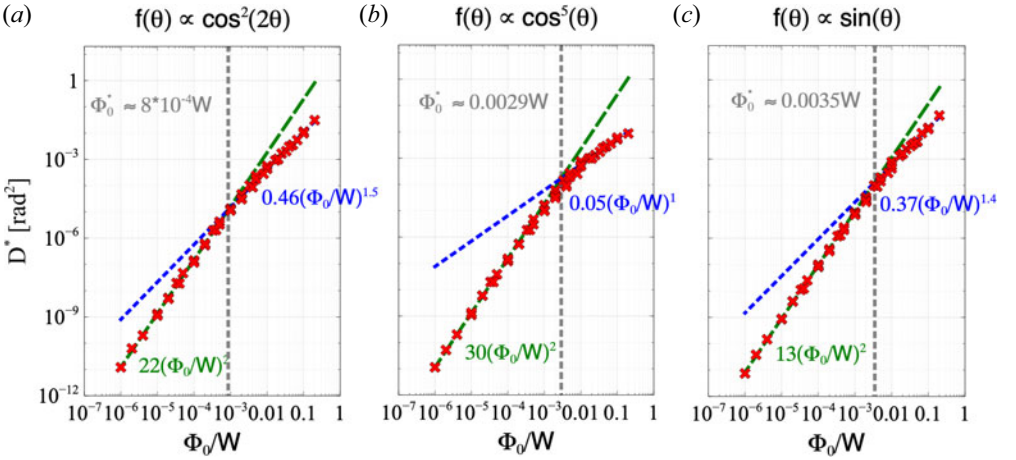

FIGURE 6. The diffusion rate D^* computed for different combinations of initial electron energies, $W \in [1, 100]$, and amplitudes of electrostatic wave packets, $\Phi_0 \in [10^{-4}, 0.2]$. There are in total 48 values for the Φ_0/W ratio. Panels (*a–c*) present scatter plots of the diffusion rate D^* vs the ratio of Φ_0/W obtained for different wave normal angle distributions of the wave packets, $f(\theta) \propto \cos^2(2\theta)$, $\cos^5\theta$ and $\sin\theta$. In each panel, green dotted lines represent the best power-law fit for $\Phi_0/W < 10^{-3}$, blue dotted lines stand for the best power-law fit in the range $0.01 < \Phi_0/W < 0.1$. Vertical grey dashed lines show the point where the two best fits intersect, and give the amplitude threshold Φ_0^* for the applicability of quasi-linear diffusion theory.

resemble those in figure 5 produced for electrons with an initial energy of $W = 5$. This result demonstrates that D^* indeed depends on the ratio Φ_0/W. The diffusion coefficient exhibits quasi-linear scaling $D^* \propto (\Phi_0/W)^2$ below some amplitude threshold, $\Phi_0 \lesssim \Phi_0^*$, and deviates from the quasi-linear scaling above that threshold. The wave normal angle distribution $f(\theta)$ affects the amplitude threshold as well as the dependence of D^* on Φ_0/W above the threshold. For wave packets propagating predominantly quasi-parallel to the local magnetic field, $f(\theta) \propto \cos^5\theta$, the amplitude threshold is $\Phi_0^*/W \approx 3 \times 10^{-3}$ and we have $D_* \approx D_0^*(\Phi_0/W)^\nu$ with $D_0^* \approx 0.05$ and $\nu \approx 1$ above the threshold. In the case of predominantly quasi-perpendicular propagation, $f(\theta) \propto \sin\theta$, the amplitude threshold is similar $\Phi_0^*/W \approx 3.5 \times 10^{-3}$, while the diffusion coefficient above the threshold scales differently, $D_* \approx D_0^*(\Phi_0/W)^\nu$ with $D_0^* \approx 0.37$ and $\nu \approx 1.4$. The case of wave packets propagating both quasi-parallel and quasi-perpendicular is characterized by a several times smaller amplitude threshold of $\Phi_0^*/W \approx 8 \times 10^{-4}$ but similar scaling of the diffusion coefficient above the threshold, $D_* \approx D_0^*(\Phi_0/W)^\nu$ with $D_0^* \approx 0.46$ and $\nu \approx 1.5$.

4. Discussion

We have analysed electron scattering by electrostatic fluctuations observed in the Earth's bow shock and, presumably, collisionless shocks in general. The electrostatic fluctuations in the Earth's quasi-perpendicular bow shock consist predominantly of electrostatic wave packets with wavelengths from a few tens to a few hundreds of Debye lengths, plasma frame speeds of around the ion-acoustic speed and relatively large amplitudes of the electrostatic potential of 1 %–20 % of the local electron temperature. Note that these parameters have been inferred from only several Earth bow shock crossings (Balikhin *et al.* 2005; Hull *et al.* 2006; Vasko *et al.* 2022), and whether they are representative of the Earth's quasi-perpendicular bow shock in general remains to be investigated.

https://doi.org/10.1017/S0022377824000217 Published online by Cambridge University Press

Importantly, electrostatic wave packets in the Earth's bow shock have the electric field oriented at various angles to the local magnetic field (figure 1 and Vasko *et al.* 2022). It is the oblique electric field orientation that allows electrostatic fluctuations to cause electron pitch-angle scattering. We applied the stochastic iterative mapping technique (Artemyev *et al.* 2021; Lukin *et al.* 2021) to quantify electron pitch-angle scattering by a large number of wave packets, whose parameters were adopted from observations in the Earth's bow shock. In this theoretical analysis we assumed that wave packets successively encountered by electrons have different amplitudes and wave normal angles, but their electrostatic potentials are described by (2.2) with $kl = 9$ and $k = 2\pi/20\lambda_D$. We also assumed that electron scatterings by successively encountered wave packets are not correlated, that is equivalent to the random phase approximation in the classical quasi-linear theory (Vedenov *et al.* 1962; Kennel & Engelmann 1966). Note, however, that, in contrast to the quasi-linear theory, the iterative mapping technique allowed us to take into account electron scattering through phase trapping and phase bunching (figure 2), which is not necessarily weak or quantifiable along unperturbed electron trajectories.

Using the iterative mapping technique, we modelled the long-term dynamics of electrons scattered by a large number of wave packets with different model probability distributions of the wave normal angle (figure 6). We showed that the long-term dynamics of electron ensembles is actually diffusive and computed the corresponding diffusion rate D^* averaged over initial electron pitch angles and gyrophases. We found that the diffusion rate D^* depends only on the ratio between the electron energy W and wave amplitude Φ_0 and scales with Φ_0/W in a power-law fashion. A quasi-linear scaling $D^* \propto (\Phi_0/W)^2$ is observed for wave amplitudes below some threshold, while the scattering is nonlinear above the threshold, $D^* \propto (\Phi_0/W)^\nu$ with $\nu < 2$. The amplitude threshold Φ_0^* depends on the wave normal angle distribution, but by the order of magnitude we have $\Phi_0^* \sim 10^{-3}\ W$ (figure 6). Since electrostatic waves reported in the Earth's bow shock have amplitudes of the order of 0.1–10 V (Hull *et al.* 2006; Vasko *et al.* 2022), the scattering of electrons with $W \lesssim 1$ keV can be nonlinear. We will concentrate on electron scattering below of approximately 1 keV. This is where scattering by electrostatic waves can be efficient, supplementing the scattering by high-frequency whistler waves, whose power is not sufficient for scattering $\lesssim 0.1$ keV electrons (Amano *et al.* 2020).

Using the computed diffusion rate D^* that is in units of rad^2 per interaction, we estimate the pitch-angle diffusion coefficient, $D = D^*/2\Delta t$, where $\Delta t \approx L(2W/m_e)^{-1/2}$ is the typical time between successive electron scatterings and L is the typical spatial distance between neighbouring wave packets along the local magnetic field. Note that, below, we restore physical units for all variables. The typical spatial distance L can be evaluated using the spatially averaged electric field amplitude E_w of electrostatic fluctuations (Vasko *et al.* 2018*a*; Shen *et al.* 2021; Kamaletdinov *et al.* 2022)

$$(eE_w)^\nu = L^{-1} \int \mathrm{d}\Phi_0\, P(\Phi_0) \int |\nabla \Phi|^\nu\, \mathrm{d}\zeta, \tag{4.1}$$

where the amplitude Φ_0 is in units of eV, $P(\Phi_0)$ is the probability distribution of wave packet amplitudes, $\Phi(\zeta)$ is the model electrostatic potential described by Eq. (2.2), measured in units of energy (eV). Since the pitch-angle diffusion coefficient $D = D^*/2\Delta t$ depends on wave amplitude it should be averaged over the probability distribution of wave packet amplitudes, $D \to \int \mathrm{d}\Phi_0\, P(\Phi_0)\, D = D_0^*/2\Delta t \cdot \int \mathrm{d}\Phi_0\, P(\Phi_0)\, (\Phi_0/W)^\nu$. Taking into account that (4.1) can be written as $(eE_w)^\nu = L^{-1} \int \mathrm{d}\Phi_0\, P(\Phi_0) \Phi_0^\nu \int |\nabla \phi|^\nu\, \mathrm{d}\zeta$,

https://doi.org/10.1017/S0022377824000217 Published online by Cambridge University Press

where $\phi(\zeta) = \Phi/\Phi_0 = \exp(-\zeta^2/2l^2)\cos(k\zeta)$, for the averaged diffusion coefficient, we obtain

$$D = \frac{D_0^*(eE_w/W)^\nu}{2(m_e/2W)^{1/2}\int|\nabla\phi|^\nu\,\mathrm{d}\zeta}. \tag{4.2}$$

In the case of $kl \gg 1$ we have $\int|\nabla\phi|^\nu\,\mathrm{d}\zeta \approx k^\nu l\,\Gamma(1/2+\nu/2)/\Gamma(1+\nu/2)(\nu/2)^{1/2} \approx 2k^\nu l/\nu$, where we have taken into account that $\xi^{1/2}\Gamma(1+\xi)/\Gamma(1/2+\xi) \approx \xi$ for $\xi \gg 0.1$. Thus, the diffusion coefficient can be written in the form

$$D \approx \frac{\nu D_0^*}{4}\left(\frac{eE_w}{kW}\right)^\nu \frac{(2W/m_e)^{1/2}}{l}, \tag{4.3}$$

clearly demonstrating that the scattering is nonlinear, because $D \propto E_w^\nu$ with $\nu < 2$. Note that the spatially averaged amplitude E_w is challenging to estimate in the Earth's bow shock but we assume it to be of the order of a temporally averaged amplitude that can be easily estimated aboard spacecraft.

The diffusion coefficient (4.3) can be expressed in a form more convenient for observations

$$D = \frac{\omega_{\mathrm{pe}}\nu D_0^*\,\varepsilon^{\nu/2}}{2^{3/2}(k\lambda_D)^{\nu-1}kl}\left(\frac{T_e}{W}\right)^{\nu-1/2}, \tag{4.4}$$

where $\varepsilon = E_w^2/4\pi n_e T_e$ is the normalized intensity of electrostatic fluctuations that was previously estimated and found to be $\varepsilon \approx 10^{-6}$–$10^{-2}$ for approximately ten Earth bow shock crossings (Kamaletdinov *et al.* 2022). Assuming $k\lambda_D = 2\pi/20$, $kl = 9$, a typical plasma density of 30 cm^{-3} and an intensity of electrostatic fluctuations of $\varepsilon \approx 10^{-6}$–$10^{-2}$, we obtain the typical values of the pitch-angle diffusion coefficient of $D \sim 0.1$–$100\,T_e/W$ $\mathrm{rad}^2\,\mathrm{s}^{-1}$ in the case of $D_0^* \approx 0.4$ and $\nu \approx 1.5$ (figure 6(*a*,*c*) and $D \sim 0.1$–$100\,(T_e/W)^{1/2}$ $\mathrm{rad}^2\,\mathrm{s}^{-1}$ in the case of $D_0^* \approx 0.05$ and $\nu \approx 1$ (figure 6*b*). Above a few keV these scattering rates are well below the pitch-angle scattering rate of 100 $\mathrm{rad}^2\,\mathrm{s}^{-1}$ reported for whistler-mode waves in the Earth's quasi-perpendicular bow show by Amano *et al.* (2020), but below approximately 1 keV the efficiency of electron scattering by the electrostatic fluctuations can be comparable to that of whistler-mode waves. Note that electron scattering rates by whistler-mode waves and electrostatic fluctuations may strongly depend on macroscopic shock parameters, but for comparative purposes we have used the estimates obtained for whistler-mode waves in one specific Earth bow shock crossing (Amano *et al.* 2020).

In the SSDA mechanism a combination of the shock drift acceleration and pitch-angle scattering of electrons in a shock transition region allows electron acceleration from lower energies up to the maximum energy W_{max} determined by the pitch-angle diffusion coefficient D in the plasma rest frame (Amano *et al.* 2020)

$$W_{\mathrm{max}} \approx 6\eta \cdot \frac{m_e V_n^2}{2\cos^2\theta_{\mathrm{Bn}}}\frac{D}{\omega_{\mathrm{ci}}}, \tag{4.5}$$

where V_n is the upstream plasma flow velocity in the normal incidence frame, θ_{Bn} is the angle between the upstream magnetic field and shock normal, ω_{ci} is the upstream ion cyclotron frequency and η is a numerical factor of the order of one. Amano *et al.* (2020) showed that the SSDA mechanism with pitch-angle scattering provided by whistler-mode waves can result in acceleration of electrons from thermal energies of approximately a hundred eV to a few tens of keV. In turn, our estimates show that the electrostatic fluctuations can also provide a substantial contribution to pitch-angle scattering of

https://doi.org/10.1017/S0022377824000217 Published online by Cambridge University Press

$\lesssim$1 keV electrons in the Earth's bow shock. We can estimate the maximum energy to which electrons are accelerated through the SSDA mechanism, assuming that pitch-angle scattering is caused solely by electrostatic fluctuations. Using the diffusion coefficient given by (4.4) we resolve (4.5) with respect to the maximum energy $W_{\max}$ and obtain the following estimate:

$$\frac{W_{\max}}{T_e} \approx \frac{\varepsilon^{\nu/(1+2\nu)}}{|\cos\theta_{\rm Bn}|^{4/(1+2\nu)}} \left[\frac{V_n^2}{c_s^2}\frac{\omega_{\rm pe}}{\omega_{\rm ce}}\frac{\eta\nu D_0^*}{(k\lambda_D)^{\nu-1}\,kl}\right]^{2/(1+2\nu)}, \tag{4.6}$$

where $c_s = (T_e/m_i)^{1/2}$ is the typical ion-acoustic speed. Taking into account that, in the Earth's bow shock we typically have $\omega_{\rm pe}/\omega_{\rm ce} \sim 100$, $V_n/c_s \sim 3$–10, $\varepsilon \sim 10^{-6}$–10^{-2} and using D_0^* and ν shown in figure 6 we obtain the following estimates:

$$\left.\begin{aligned} \frac{W_{\max}}{T_e} &\approx \frac{15\varepsilon^{3/8}}{|\cos\theta_{\rm Bn}|} \sim \frac{0.05-5}{|\cos\theta_{\rm Bn}|}, \\ \frac{W_{\max}}{T_e} &\approx \frac{5\varepsilon^{1/3}}{|\cos\theta_{\rm Bn}|^{4/3}} \sim \frac{0.05-1}{|\cos\theta_{\rm Bn}|^{4/3}}, \end{aligned}\right\} \tag{4.7}$$

where the first estimate was obtained using $D_0^* \approx 0.4$ and $\nu \approx 1.5$ (figure 6*a*,*c*), while the second one was obtained using $D_0^* \approx 0.05$ and $\nu \approx 1$ (figure 6*b*).

Since in the Earth's bow shock $T_e \sim 10$–100 eV, (4.7) show that the electrostatic fluctuations can contribute to the acceleration of thermal electrons with $W \ll T_e$ up to $W_{\max} \sim 10T_e \sim 100$ eV–1 keV. We conclude that non-adiabatic electron heating (Gedalin *et al.* 2023; Johlander *et al.* 2023) and increased fluxes of superthermal electrons (Gosling *et al.* 1989; Oka *et al.* 2006) reported in the Earth's quasi-perpendicular bow shock can be at least partially caused by scattering due to the electrostatic fluctuations. A thorough statistical analysis of waves in the Earth's bow shock is required to quantify the contribution of different waves to electron scattering. The theoretical estimates presented here only allow us to propose that electrostatic fluctuations observed in the Earth's bow shock may cause substantial scattering of $\lesssim$1 keV electrons and that they are not likely to compete with whistler-mode waves above a few keV. However, it is important to note that our theoretical estimates and discussion have been based on just a few Earth bow shock crossings considered by Amano *et al.* (2020) and Vasko *et al.* (2022), while the properties of electrostatic fluctuations and whistler-mode waves may strongly depend on macroscopic shock parameters.

Several comments are in order about the presented estimates. First, we used a fixed ratio between electron cyclotron and plasma frequencies, $\Omega = \omega_{\rm ce}/\omega_{\rm pe} = 10^{-2}$, that is, typical of the Earth's bow shock (see, e.g. Kamaletdinov *et al.* 2022). We expect this parameter to affect the diffusion coefficient, because even the quasi-liner diffusion coefficient depends on Ω (see equation (14) in Kamaletdinov *et al.* (2022) obtained for electron scattering by electrostatic solitary waves). The dependence of the nonlinear diffusion coefficient D^* on Ω, where the latter parameter is typically in the range between 10^{-3} and 10^{-1}, needs to be quantified in the future. Second, we assumed electrostatic wave packets to have a planar wavefront or, equivalently, infinite perpendicular coherence scale. We expect a finite coherence scale to limit the efficiency of nonlinear interaction (trapping and bunching) and actually extend the applicability of quasi-linear theory to lower energies, but we leave the corresponding analysis for future studies. Third, we considered the case of wave packets with zero phase speed in the plasma frame, so that no energy diffusion occurs in that frame. In reality, the plasma frame speed of electrostatic wave packets in the Earth's bow shock is

https://doi.org/10.1017/S0022377824000217 Published online by Cambridge University Press

of the order of the ion-acoustic speed (figure 1), and some energy diffusion actually occurs. This energy diffusion can be directly related to the pitch-angle diffusion, since, during interaction with each wave packet, electron energy in the wave packet's frame conserves, $(V_\parallel - V_s/\cos\theta)^2 + V_\perp^2 = \text{const.}$, where V_s is the phase speed of the wave packet. Using the energy conservation condition we relate energy and pitch-angle variations, $\Delta W/W = 2V_s \sin\alpha/(V_s\cos\alpha - V\cos\theta)\Delta\alpha$ (Lyons 1974; Vasko *et al.* 2018*a*; Kamaletdinov *et al.* 2022). Since the speed of wave packets in the Earth's bow shock is much smaller than the speed of thermal and superthermal electrons, $V_s \ll V$, the energy diffusion can be actually neglected, $\Delta W^2/W^2 \approx 4(V_s \sin\alpha/V\cos\theta)^2\Delta\alpha^2 \ll \Delta\alpha^2$.

Finally, we note that the presented results may have other potential applications. First, a similar methodology can be applied to quantify electron heating and acceleration in astrophysical shocks, including those in supernova remnants and galaxy clusters, although in this case the properties of electrostatic fluctuations need to be adopted from theory or simulations. Note that Buneman and ion-acoustic fluctuations are highly likely excited in astrophysical shocks according to numerical simulations (e.g. Cargill & Papadopoulos 1988; Amano & Hoshino 2009). Second, similar electrostatic fluctuations have been observed in other space plasma environments, including the solar wind (Gurnett & Frank 1978; Mozer *et al.* 2020), the Earth's magnetosheath (Rodriguez 1979; Mangeney *et al.* 2006), the auroral region (Mozer *et al.* 1979; Temerin *et al.* 1981), the inner magnetosphere (Mozer *et al.* 2015; Vasko *et al.* 2017) as well as reconnecting current sheets at the Earth's magnetopause and magnetotail (Graham *et al.* 2016; Liu *et al.* 2019; Wang *et al.* 2022). The presented methodology can be used to quantify electron pitch-angle scattering and associated heating and acceleration in these environments.

5. Conclusions

In this paper we used the iterative mapping technique to model pitch-angle scattering of electrons by a large number of wave packets that have been observed in the Earth's bow shock. In this technique, the successive electron scatterings are not correlated, while the scattering of individual electrons can be nonlinear and occurs through phase trapping and phase bunching. The results of this study can be summarized as follows:

(i) Even though the scattering of individual electrons can be nonlinear, the long-term dynamics of electron ensembles scattered by a larger number of wave packets is diffusive.

(ii) The diffusion rate D^* that is in units of rad^2 per interaction depends only on the ratio between the electron energy and the wave amplitude, $D^* \approx D_0^*(\Phi_0/W)^\nu$, where parameters D_0^* and ν depend on the wave normal angle distribution of the wave packets. A quasi-linear scaling ($\nu \approx 2$) is observed for sufficiently small wave amplitudes, $\Phi_0 \lesssim 10^{-3}\ W$, while the diffusion is nonlinear ($\nu < 2$) above this threshold.

(iii) The pitch-angle diffusion coefficient in units of rad^2 s^{-1} corresponding to the revealed diffusion rate is given by (4.3) and (4.4). In the Earth's bow shock, the scattering of electrons below approximately 1 keV can be nonlinear and the diffusion coefficient may depend on the intensity of electrostatic fluctuations in a nonlinear fashion, $D \propto E_w^\nu$ with $\nu < 2$. The typical values of the diffusion coefficient of $\lesssim$1 keV electrons are $D \sim 0.1$–$100\ (T_e/W)^{\nu-1/2}$ rad^2 s^{-1}.

(iv) The SSDA mechanism with pitch-angle scattering provided solely by the electrostatic fluctuations can provide acceleration of thermal electrons up to the maximum energy given by (4.7). In the Earth's quasi-perpendicular bow shock the maximum energy can be as large as approximately 1 keV.

https://doi.org/10.1017/S0022377824000217 Published online by Cambridge University Press

Acknowledgements

We would like to thank MMS teams for the excellent data. All the data used in this study are publicly available at https://lasp.colorado.edu/mms/sdc/public/.

Editor A.C. Bret thanks the referees for their advice in evaluating this article.

Funding

This work of I.V. was supported by NASA grants No. 80NSSC21K0730 and 80NSSC20K1325. S.K. acknowledges support from Russian Science Foundation through grant No. 19-12-00313 covering the theoretical part of this work.

Declaration of interests

The authors report no conflict of interest.

REFERENCES

ALBERT, J.M., MEREDITH, N.P. & HORNE, R.B. 2009 Three-dimensional diffusion simulation of outer radiation belt electrons during the 9 October 1990 magnetic storm. *J. Geophys. Res.* **114**, 9214.

AMANO, T. & HOSHINO, M. 2009 Nonlinear evolution of Buneman instability and its implication for electron acceleration in high Mach number collisionless perpendicular shocks. *Phys. Plasmas* **16** (10), 102901.

AMANO, T., KATOU, T., KITAMURA, N., OKA, M., MATSUMOTO, Y., HOSHINO, M., SAITO, Y., YOKOTA, S., GILES, B.L., PATERSON, W.R., *et al.* 2020 Observational evidence for stochastic shock drift acceleration of electrons at the Earth's bow shock. *Phys. Rev. Lett.* **124** (6), 065101.

AMANO, T., MATSUMOTO, Y., BOHDAN, A., KOBZAR, O., MATSUKIYO, S., OKA, M., NIEMIEC, J., POHL, M. & HOSHINO, M. 2022 Nonthermal electron acceleration at collisionless quasi-perpendicular shocks. *Rev. Mod. Plasma Phys.* **6** (1), 29.

ARTEMYEV, A.V., NEISHTADT, A.I., VASILIEV, A.A. & MOURENAS, D. 2016 Kinetic equation for nonlinear resonant wave-particle interaction. *Phys. Plasmas* **23** (9), 090701.

ARTEMYEV, A.V., NEISHTADT, A.I., VASILIEV, A.A. & MOURENAS, D. 2021 Transitional regime of electron resonant interaction with whistler-mode waves in inhomogeneous space plasma. *Phys. Rev.* E **104** (5), 055203.

ARTEMYEV, A.V., SHI, X., LIU, T.Z., ZHANG, X.J., VASKO, I. & ANGELOPOULOS, V. 2022 Electron resonant interaction with whistler waves around foreshock transients and the bow shock behind the terminator. *J. Geophys. Res.* **127** (2), e29820.

BALIKHIN, M., WALKER, S., TREUMANN, R., ALLEYNE, H., KRASNOSELSKIKH, V., GEDALIN, M., ANDRE, M., DUNLOP, M. & FAZAKERLEY, A. 2005 Ion sound wave packets at the quasiperpendicular shock front. *Geophys. Res. Lett.* **32** (24), L24106.

BRENEMAN, A.W., CATTELL, C.A., KERSTEN, K., PARADISE, A., SCHREINER, S., KELLOGG, P.J., GOETZ, K. & WILSON, L.B. 2013 STEREO and Wind observations of intense cyclotron harmonic waves at the Earth's bow shock and inside the magnetosheath. *J. Geophys. Res.* **118** (12), 7654–7664.

BURCH, J.L., MOORE, T.E., TORBERT, R.B. & GILES, B.L. 2016 Magnetospheric multiscale overview and science objectives. *Space Sci. Rev.* **199**, 5–21.

CARGILL, P.J. & PAPADOPOULOS, K. 1988 A mechanism for strong shock electron heating in supernova remnants. *Astrophys. J. Lett.* **329**, L29.

ERGUN, R.E., TUCKER, S., WESTFALL, J., GOODRICH, K.A., MALASPINA, D.M., SUMMERS, D., WALLACE, J., KARLSSON, M., MACK, J., BRENNAN, N., *et al.* 2016 The axial double probe and fields signal processing for the MMS mission. *Space Sci. Rev.* **199**, 167–188.

FUSELIER, S.A. & GURNETT, D.A. 1984 Short wavelength ion waves upstream of the Earth's bow shock. *J. Geophys. Res.* **89** (A1), 91–104.

GEDALIN, M. 2020 Large-scale versus small-scale fields in the shock front: effect on the particle motion. *Astrophys. J.* **895** (1), 59.

GEDALIN, M., GOLAN, M., VINK, J., GANUSHKINA, N. & BALIKHIN, M. 2023 Electron heating in shocks: statistics and comparison. *J. Geophys. Res*. **128** (9), e2023JA031627.

GHAVAMIAN, P., SCHWARTZ, S.J., MITCHELL, J., MASTERS, A. & LAMING, J.M. 2013 Electron-ion temperature equilibration in collisionless shocks: the supernova remnant-solar wind connection. *Space Sci. Rev*. **178** (2–4), 633–663.

GOSLING, J.T., THOMSEN, M.F., BAME, S.J. & RUSSELL, C.T. 1989 Suprathermal electrons at Earth's bow shock. *J. Geophys. Res*. **94** (A8), 10011–10025.

GRAHAM, D.B., KHOTYAINTSEV, Y.V., VAIVADS, A. & ANDRÉ, M. 2016 Electrostatic solitary waves and electrostatic waves at the magnetopause. *J. Geophys. Res*. **121** (4), 3069–3092.

GURNETT, D.A. 1985 *Plasma Waves and Instabilities*. Geophysical Monograph Series, vol. 35, pp. 207–224. American Geophysical Union.

GURNETT, D.A. & FRANK, L.A. 1978 Ion acoustic waves in the solar wind. *J. Geophys. Res*. **83** (A1), 58–74.

HULL, A.J., LARSON, D.E., WILBER, M., SCUDDER, J.D., MOZER, F.S., RUSSELL, C.T. & BALE, S.D. 2006 Large-amplitude electrostatic waves associated with magnetic ramp substructure at Earth's bow shock. *Geophys. Res. Lett*. **33** (15), L15104.

JOHLANDER, A., KHOTYAINTSEV, Y.V., DIMMOCK, A.P., GRAHAM, D.B. & LALTI, A. 2023 Electron heating scales in collisionless shocks measured by MMS. *Geophys. Res. Lett*. **50** (5), e2022GL100400.

KAMALETDINOV, S., VASKO, I., ARTEMYEV, A., WANG, R. & MOZER, F. 2022 Quantifying electron scattering by electrostatic solitary waves in the Earth's bow shock. *Phys. Plasmas* **29** (8), 082301.

KAMALETDINOV, S.R., VASKO, I.Y., WANG, R., ARTEMYEV, A.V., YUSHKOV, E.V. & MOZER, F.S. 2022 Slow electron holes in the Earth's bow shock. *Phys. Plasmas* **29** (9), 092303.

KENNEL, C.F. & ENGELMANN, F. 1966 Velocity space diffusion from weak plasma turbulence in a magnetic field. *Phys. Fluids* **9**, 2377–2388.

KRASNOSELSKIKH, V., BALIKHIN, M., WALKER, S.N., SCHWARTZ, S., SUNDKVIST, D., LOBZIN, V., GEDALIN, M., BALE, S.D., MOZER, F., SOUCEK, J., *et al.* 2013 The dynamic quasiperpendicular shock: cluster discoveries. *Space Sci. Rev*. **178**, 535–598.

LALTI, A., KHOTYAINTSEV, Y.V., GRAHAM, D.B., VAIVADS, A., STEINVALL, K. & RUSSELL, C.T. 2022 Whistler waves in the foot of quasi-perpendicular supercritical shocks. *J. Geophys. Res*. **127** (5), e2021JA029969.

LINDQVIST, P.-A., OLSSON, G., TORBERT, R.B., KING, B., GRANOFF, M., RAU, D., NEEDELL, G., TURCO, S., DORS, I., BECKMAN, P., *et al.* 2016 The spin-plane double probe electric field instrument for MMS. *Space Sci. Rev*. **199**, 137–165.

LIU, C.M., VAIVADS, A., GRAHAM, D.B., KHOTYAINTSEV, Y.V., FU, H.S., JOHLANDER, A., ANDRÉ, M. & GILES, B.L. 2019 Ion-beam-driven intense electrostatic solitary waves in reconnection jet. *Geophys. Res. Lett*. **46** (22), 12702–12710.

LUKIN, A.S., ARTEMYEV, A.V. & PETRUKOVICH, A.A. 2021 On application of stochastic differential equations for simulation of nonlinear wave-particle resonant interactions. *Phys. Plasmas* **28** (9), 092904.

LYONS, L.R. 1974 Pitch angle and energy diffusion coefficients from resonant interactions with ion-cyclotron and whistler waves. *J. Plasma Phys*. **12**, 417–432.

MANGENEY, A., LACOMBE, C., MAKSIMOVIC, M., SAMSONOV, A.A., CORNILLEAU-WEHRLIN, N., HARVEY, C.C., BOSQUED, J.M. & TRÁVNÍČEK, P. 2006 Cluster observations in the magnetosheath. Part 1. Anisotropies of the wave vector distribution of the turbulence at electron scales. *Ann. Geophys*. **24** (12), 3507–3521.

MARKEVITCH, M. & VIKHLININ, A. 2007 Shocks and cold fronts in galaxy clusters. *Phys. Rep*. **443** (1), 1–53.

MOZER, F.S., AGAPITOV, O., ARTEMYEV, A., DRAKE, J.F., KRASNOSELSKIKH, V., LEJOSNE, S. & VASKO, I. 2015 Time domain structures: what and where they are, what they do, and how they are made. *Geophys. Res. Lett*. **42**, 3627–3638.

MOZER, F.S., BONNELL, J.W., BOWEN, T.A., SCHUMM, G. & VASKO, I.Y. 2020 Large-amplitude, wideband, Doppler-shifted, ion acoustic waves observed on the parker solar probe. *Astrophys. J*. **901** (2), 107.

https://doi.org/10.1017/S0022377824000217 Published online by Cambridge University Press

MOZER, F.S., CATTELL, C.A., TEMERIN, M., TORBERT, R.B., VON GLINSKI, S., WOLDORFF, M. & WYGANT, J. 1979 The DC and AC electric field, plasma density, plasma temperature, and field-aligned current experiments on the S3-3 satellite. *J. Geophys. Res*. **84**, 5875–5884.

MUSCHIETTI, L. & LEMBÈGE, B. 2017 Two-stream instabilities from the lower-hybrid frequency to the electron cyclotron frequency: application to the front of quasi-perpendicular shocks. *Ann. Geophys*. **35** (5), 1093–1112.

NEISHTADT, A.I., CHAIKOVSKII, D.K. & CHERNIKOV, A.A. 1991 Adiabatic chaos and diffusion of particles. *Zh. Eksp. Teor. Fiz*. **99**, 763–776.

NUNN, D. 1971 Wave-particle interactions in electrostatic waves in an inhomogeneous medium. *J. Plasma Phys*. **6**, 291.

OKA, M., OTSUKA, F., MATSUKIYO, S., WILSON, L.B. III, Argall, M.R., Amano, T., Phan, T.D., Hoshino, M., Le Contel, O., Gershman, D.J., *et al.* 2019 Electron scattering by low-frequency whistler waves at Earth's bow shock. *Astrophys. J*. **886** (1), 53.

OKA, M., TERASAWA, T., SEKI, Y., FUJIMOTO, M., KASABA, Y., KOJIMA, H., SHINOHARA, I., MATSUI, H., MATSUMOTO, H., SAITO, Y., *et al.* 2006 Whistler critical Mach number and electron acceleration at the bow shock: geotail observation. *Geophys. Res. Lett*. **33** (24), L24104.

OKA, M., WILSON, L.B. III, PHAN, T.D., HULL, A.J., AMANO, T., HOSHINO, M., ARGALL, M.R., LE CONTEL, O., AGAPITOV, O., GERSHMAN, D.J., *et al.* 2017 Electron scattering by high-frequency whistler waves at Earth's bow shock. *Astrophys. J. Lett*. **842**, L11.

OMURA, Y., MATSUMOTO, H., NUNN, D. & RYCROFT, M.J. 1991 A review of observational, theoretical and numerical studies of VLF triggered emissions. *J. Atmos. Terr. Physi*. **53**, 351–368.

OMURA, Y., MIYASHITA, Y., YOSHIKAWA, M., SUMMERS, D., HIKISHIMA, M., EBIHARA, Y. & KUBOTA, Y. 2015 Formation process of relativistic electron flux through interaction with chorus emissions in the Earth's inner magnetosphere. *J. Geophys. Res*. **120**, 9545–9562.

PAGE, B., VASKO, I.Y., ARTEMYEV, A.V. & BALE, S.D. 2021 Generation of high-frequency whistler waves in the Earth's quasi-perpendicular bow shock. *Astrophys. J. Lett*. **919** (2), L17.

POLLOCK, C., MOORE, T., JACQUES, A., BURCH, J., GLIESE, U., SAITO, Y., OMOTO, T., AVANOV, L., BARRIE, A., COFFEY, V., *et al.* 2016 Fast plasma investigation for magnetospheric multiscale. *Space Sci. Rev*. **199**, 331–406.

RAYMOND, J.C., GHAVAMIAN, P., BOHDAN, A., RYU, D., NIEMIEC, J., SIRONI, L., TRAN, A., AMATO, E., HOSHINO, M., POHL, M., *et al.* 2023 Electron-ion temperature ratio in astrophysical shocks. *Astrophys. J*. **949** (2), 50.

RODRIGUEZ, P. 1979 Magnetosheath electrostatic turbulence. *J. Geophys. Res*. **84** (A3), 917–930.

RUSSELL, C.T., ANDERSON, B.J., BAUMJOHANN, W., BROMUND, K.R., DEARBORN, D., FISCHER, D., LE, G., LEINWEBER, H.K., LENEMAN, D., MAGNES, W., *et al.* 2016 The magnetospheric multiscale magnetometers. *Space Sci. Rev*. **199**, 189–256.

SCUDDER, J.D. 1995 A review of the physics of electron heating at collisionless shocks. *Adv. Space Res*. **15**, 181–223.

SHEN, Y., VASKO, I.Y., ARTEMYEV, A., MALASPINA, D.M., CHU, X., ANGELOPOULOS, V. & ZHANG, X.-J. 2021 Realistic electron diffusion rates and lifetimes due to scattering by electron holes. *J. Geophys. Res*. **126** (9), e29380.

SHKLYAR, D.R. & MATSUMOTO, H. 2009 Oblique whistler-mode waves in the inhomogeneous magnetospheric plasma: resonant interactions with energetic charged particles. *Surv. Geophys*. **30**, 55–104.

TEMERIN, M., CATTELL, C., LYSAK, R., HUDSON, M., TORBERT, R.B., MOZER, F.S., SHARP, R.D. & KINTNER, P.M. 1981 The small-scale structure of electrostatic shocks. *J. Geophys. Res*. **86** (A13), 11278–11298.

VASKO, I.Y., AGAPITOV, O.V., MOZER, F.S., ARTEMYEV, A.V., KRASNOSELSKIKH, V.V. & BONNELL, J.W. 2017 Diffusive scattering of electrons by electron holes around injection fronts. *J. Geophys. Res*. **122**, 3163–3182.

VASKO, I.Y., KRASNOSELSKIKH, V.V., MOZER, F.S. & ARTEMYEV, A.V. 2018*a* Scattering by the broadband electrostatic turbulence in the space plasma. *Phys. Plasmas* **25** (7), 072903.

VASKO, I.Y., MOZER, F.S., BALE, S.D. & ARTEMYEV, A.V. 2022 Ion-acoustic waves in a quasi-perpendicular Earth's bow shock. *Geophys. Res. Lett*. **49** (11), e98640.

VASKO, I.Y., MOZER, F.S., KRASNOSELSKIKH, V.V., ARTEMYEV, A.V., AGAPITOV, O.V., BALE, S.D., AVANOV, L., ERGUN, R., GILES, B., LINDQVIST, P.-A., *et al.* 2018*b* Solitary waves across supercritical quasi-perpendicular shocks. *Geophys. Res. Lett*. **45**, 5809–5817.

VASKO, I.Y., WANG, R., MOZER, F.S., BALE, S.D. & ARTEMYEV, A.V. 2020 On the nature and origin of bipolar electrostatic structures in the Earth's bow shock. *Front. Phys*. **8**, 156.

VEDENOV, A.A., VELIKHOV, E. & SAGDEEV, R. 1962 Quasilinear theory of plasma oscillations. *Nucl. Fusion Suppl*. **2**, 465–475.

WALT, M. 1994 *Introduction to geomagnetically trapped radiation*. Camb. Atmos. Space Sci. Ser. Cambridge University Press.

WANG, R., VASKO, I.Y., ARTEMYEV, A.V., HOLLEY, L.C., KAMALETDINOV, S.R., LOTEKAR, A. & MOZER, F.S. 2022 Multisatellite observations of ion holes in the Earth's plasma sheet. *Geophys. Res. Lett*. **49** (8), e97919.

WANG, R., VASKO, I.Y., MOZER, F.S., BALE, S.D., ARTEMYEV, A.V., BONNELL, J.W., ERGUN, R., GILES, B., LINDQVIST, P.A., RUSSELL, C.T., *et al.* 2020 Electrostatic turbulence and Debye-scale structures in collisionless shocks. *Astrophys. J. Lett*. **889** (1), L9.

WANG, R., VASKO, I.Y., MOZER, F.S., BALE, S.D., KUZICHEV, I.V., ARTEMYEV, A.V., STEINVALL, K., ERGUN, R., GILES, B., KHOTYAINTSEV, Y., *et al.* 2021 Electrostatic solitary waves in the Earth's bow shock: nature, properties, lifetimes, and origin. *J. Geophys. Res*. **126** (7), e29357.

WILSON, L.B., SIBECK, D.G., BRENEMAN, A.W., CONTEL, O.L., CULLY, C., TURNER, D.L., ANGELOPOULOS, V. & MALASPINA, D.M. 2014 Quantified energy dissipation rates in the terrestrial bow shock: 2. Waves and dissipation. *J. Geophys. Res*. **119**, 6475–6495.

ZHANG, X.-J., ARTEMYEV, A., ANGELOPOULOS, V., TSAI, E., WILKINS, C., KASAHARA, S., MOURENAS, D., YOKOTA, S., KEIKA, K., HORI, T., *et al.* 2022 Superfast precipitation of energetic electrons in the radiation belts of the Earth. *Nat. Commun*. **13**, 1611.

https://doi.org/10.1017/S0022377824000217 Published online by Cambridge University Press